The New Celebration Gold Deposits: Characteristics and Evolution of Hydrothermal Fluids

JOANNA L. HODGE, STEFFEN G. HAGEMANN AND PETER NEUMAYR
Centre for Global Metallogeny, University of Western Australia, Crawley, WA 6009

Introduction

Archean orogenic lode-gold deposits world-wide, typically show a close spatial association with first-order, trans-crustal fault systems ((Eisenlohr et al., 1989; Neumayr et al., 2000). At a camp- to deposit-scale, however, second- and third-order splays host the majority of world class (>100t Au) orogenic lode gold deposits (Eisenlohr et al., 1989; Groves et al., 1990). While much research into the fluid chemistry and P-T-X-t evolution of hydrothermal fluids in the gold-endowed second- and third-order fault systems has been undertaken, first-order faults have been largely ignored. This is mainly due to the fact that most first-order fault systems are barren and research has focused on mineralised lower-order faults adjacent to the main trans-crustal faults, but is also due to the poor exposure of first-order faults. Recent work on first-order structures has focused on the structure (Robert, 1989; Wilkinson et al., 1999), timing of mineralisation (Neumayr et al., 2000; Robert, 1990) and hydrothermal fluid evolution (Neumayr and Hagemann, 2002) on the Cadillac Tectonic Zone in the Abitibi greenstone belt, but until now, very little work has occurred on similar structures in the Yilgarn craton of Western Australia.

The Boulder-Lefroy fault zone (BLFZ) is an interpreted, first-order trans-crustal fault zone located in the Eastern Goldfields Province of the Yilgarn Craton (Swager, 1989). It is spatially correlated with the Golden Mile and St Ives world-class gold camps, both of which are hosted in adjacent second- and third-order splays. The BLFZ also hosts the New Celebration gold deposit. Previous workers have focused on the structural controls (Dielemans, 2000) and lithological controls (Williams, 1994) of Southern Ore Zone mineralisation at New Celebration, while more recently, Nichols (2003) and Nichols et al. (in prep) evaluated the structural controls, hydrothermal alteration and timing of mineralisation of the entire New Celebration gold system. Given that orogenic gold deposits hosted in first-order fault systems are rare, the New Celebration gold deposit provides a unique opportunity to study the fluid P-T-X-t evolution in a first-order fault system, and evaluate the role regional scale structures play in focusing mineralising and non-mineralising fluids. This study aims to assess the paleohydrologic regime at New Celebration by: 1) characterising the vein system and establishing a vein paragenesis with respect to deformation and mineralisation; 2) evaluating the P-T-X-t fluid characteristics of the fluid inclusions trapped in veins in the context of deformation and mineralisation; 3) constraining the P-T-X evolution of the fluids through time; and 4) developing a hydrothermal fluid evolution model at New Celebration.

The aim of this report is to present results of the preliminary investigations into the hydrothermal fluid system at New Celebration and to constrain the P-T-X-t conditions of fluids associated with deformation, hydrothermal alteration and gold mineralisation. A preliminary model of hydrothermal fluid evolution through time is presented and constraints on the gold deposition evaluated.

Regional Geology

The Kalgoorlie Terrane is a 6-9km thick, elongate volcano-sedimentary sequence which is bounded to the east and west by wide (up to 1km) anastamosing shear zones (Swager, 1997). The sequence comprises a lower basalt unit conformably overlain by komatiite and interflow sediments, an upper basalt unit and felsic volcanic and volcaniclastic rocks, and is intruded by a number of different granitoid suites. Coarse clastic basins are the youngest rocks, which unconfomably overlie the greenstone sequence and commonly bury major boundary faults (Swager, 1997). Regionally the terrane is metamorphosed to upper greenschist facies, with locally higher metamorphic grades (up to amphibolite facies) recorded along the margins (Binns et al., 1976; Witt, 1991). Four main compressive episodes are recognised in the Kalgoorlie Terrane, preceded by a periods of extension (Swager and Nelson, 1997). The volcano-sedimentary sequence was deposited during the earliest extensional phase (Passchier, 1994; Williams and Currie, 1993) and was followed by D1, a period of south over north compression, which resulted in widespread structural

repetition and thrust faulting (Swager and Nelson, 1997). A second extensional phase followed, in which the coarse clastic sequences were deposited and accompanied by widespread granitoid intrusion occurred (Weinberg et al., 2003). Regional D2 shortening was approximately E-W and resulted in NNW-SSE trending upright folds and penetrative foliation (Swager, 1989; Swager and Griffin, 1990; Weinberg et al., 2003). During D3 and D4 deformation became strike-slip in nature and progressed from a ductile to a brittle regime (Bateman et al., 2001; Mueller et al., 1988; Swager, 1997).

Geological Setting of the New Celebration Gold Deposits

The following review is taken from Nichols (2003) and Nichols et al. (in prep, contained in this report).

Structural Setting and Deformation Events

The New Celebration gold deposits are hosted within a sequence of ultramafic (Kambalda Komatiite) and differentiated mafic (Pernatty Dolerite) rocks, which have been intruded by several generations of felsic and lamprophyric dykes. The units are folded; to the west of the BLFZ the sequence youngs west, while on the eastern side of the fault it is east younging (N.J. Archibald, unpub. report, 1992)

Nichols (2003) identified three main deformation events at New Celebration, and tentatively correlated them with regional deformation events. For clarity Nichols (2003) identified the local New Celebration events with the subscript $_{NC}$ and denoted the first deformation event as D2 as it is tentatively correlated with regional D2. An event correlating to regional D1 was not recognised at the New Celebration gold deposit. The earliest recognised deformation event at New Celebration ($D2_{NC}$) is characterised by conformable stratigraphic contacts which have been tilted to vertical and corresponds to the upright folding of Swager (1990) and Swager and Griffin (1990). $D3_{NC}$ is represented by a NNW-trending shear foliation in mafic and ultramafic rocks, well-developed S (82° towards 260°) and C (87° towards 229°) fabrics in mafic rocks and foliated porphyry dykes and mineral elongations, S-C intersection lineations and slickenline lineations observed in the open pit. $D3_{NC}$ tentatively correlates with regional D3 ENE-WSW compression and sinistral strike- and dip-slip faulting (Swager, 1989; Swager and Griffin, 1990). North-northwest dipping structures and a second penetrative S-C fabric, oriented 81° towards 312 and 58° towards 292°, cross-cut $S3_{NC}$ represent $D4_{NC}$. Late curviplanar faults that crosscut all other structures are assigned to $D4_{NC}$.

Nichols (2003) recognised two major magmatic events at New Celebration, based on mineralogy, deformation style and crosscutting relationships. Early intensely altered plagioclase porphyries are denoted M1 and have a penetrative $S3_{NC}$ foliation. These intrusions are cross-cut by weakly altered, unfoliated to weakly foliated quartz-feldspar porphyries, designated M2, which preserve primary igneous textures. The M2 porphyries are boudinaged along strike and at depth, but are wrapped by $S3_{NC}$ foliation, indicating they were emplaced late during D3 deformation.

Hydrothermal Alteration and Gold Mineralisation

Based on evidence from open pit mapping, diamond core logging, detailed geochemistry and petrography, Nichols (2003) identified two gold mineralising events at New Celebration; an early event that comprises Mylonite- and Porphyry-style mineralisation, and a late event that comprises Contact- and Fracture-style mineralisation.

Early Gold Mineralisation

Mylonitised M1 porphyry hosts Mylonite-style gold mineralisation while Porphyry-style mineralisation is hosted in less deformed M1 porphyry. Gold occurs as rounded inclusions in deformed pyrite within $S3_{NC}$ foliation planes, or less commonly, along pyrite grain fractures or adjacent to pyrite along albite grain boundaries. The gold-hosting pyrite is in textural equilibrium with $S3_{NC}$ biotite foliation planes and is interpreted to have occurred syn-$D3_{NC}$. Early gold mineralisation is characterised by biotite-ankerite-sericite-pyrite alteration and a strong telluride association.

Late Gold Mineralisation

The high-Mg basalt-M2 porphyry contact hosts Contact-style gold mineralisation. Gold occurs in deformed pyrite, which is in textural equilibrium within $S3_{NC}$ foliation planes, which wrap around the M2

porphyry. Abundant coarse-grained pyrite immediately adjacent to the contact is characteristic of Contact-style mineralisation. The proximal alteration assemblage comprises ankerite-sericite. Contact-style mineralisation is not accompanied by accessory tellurides.

Thin (1-2mm) fractures developed on the margins of M2 porphyries host Fracture-style mineralisation. Pyrite hosts gold as intragranular inclusions or along grain boundaries. Proximal alteration comprises pyrite-sericite±chlorite and is restricted to the fracture fill. Fracture-style mineralisation clearly crosscuts $S3_{NC}$ fabrics and is interpreted to have occurred post-$D3_{NC}$.

Vein Paragenesis

The vein system at the New Celebration gold deposit is complex, and crosscutting relationships between early gold associated veins and late gold associated veins are not observed, however, temporal interpretations can be made based on the relative timing of the emplacement of the gold mineralised host rocks. Preliminary investigations suggest that the New Celebration vein system comprises: (1) pre-early gold event veins developed prior to $D3_{NC}$, (2) syn-early gold event veins developed during $D3_{NC}$, (3) pre-late gold event veins developed syn-late $D3_{NC}$ or post $D3_{NC}$, and (4) syn-late gold event veins possibly developed during $D4_{NC}$ (Table 1).

Veins Related to Early Mineralisation

Pre-$D3_{NC}$ Veins: The earliest observed veins at New Celebration are foliation-parallel quartz-calcite "boudins". These veins are hosted in strongly foliated, and mylonitised, M1 feldspar porphyries. Quartz and calcite grains within these veins exhibit undulose extinction and have undergone complete dynamic recrystallisation by grain boundary migration and sub-grain rotation (c.f. Passchier and Trouw, 1996) .

Syn-$D3_{NC}$ Veins: Early gold event-related veins comprise predominantly quartz and calcite with accessory pyrite and ankerite. Two vein types are observed: 1) approximately foliation parallel veins exclusively hosted by M1 feldspar porphyries, and 2) zoned quartz-calcite or calcite-only extension veins which have developed in M1 feldspar porphyries, mylonitised M1 porphyries and mafic and ultramafic schists. These veins occur perpendicular to foliation, but show mutually cross-cutting relationships with the foliation planes.

The veins are typically surrounded by wide (20-50mm) ankerite alteration zones and zoned pyrite concentrates along the vein selvedges in clusters of large, inclusion-rich grains. Pyrite grains typically exhibit a "dirty", inclusion-rich core surrounded by a "clean", inclusion free rim. Inclusions typically comprise abundant silicates, minor sulfides (galena, sphalerite) and rare gold blebs. The veins contain quartz grains that have undergone partial dynamic recrystallisation by grain boundary migration and sub-grain rotation. Grain boundaries are often highly irregular and protrude into neighbouring grains, although the degree to which individual samples have been recrystallised varies. Sub-grain development is minor and is predominantly concentrated along the outer vein edge. Relict grains locally exhibit undulose extinction and lattice-preferred orientation (c.f. Passchier and Trouw, 1996).

Veins Related to Late Mineralisation

Late/Post-$D3_{NC}$ Veins: Late/post-$D3_{NC}$ veins comprise quartz, carbonate and sericite. The veins are composed almost entirely of coarse-grained (1-5mm) clear quartz overprinted by accessory calcite and rare sericite. The veins form breccias within M2 quartz-feldspar porphyries. Quartz grains within these veins show evidence that they have undergone partial dynamic recrystallisation by grain boundary migration. This evidence includes diffuse and highly irregular grain boundaries.

$D4_{NC}$ Veins: Late-gold event-related veins are composed of sericite, chlorite and pyrite and form thin stringer veins. These veins only occur in M2 quartz-feldspar porphyries. Where the $D4_{NC}$ veins crosscut the earlier quartz breccia, they have generally developed along the quartz grain boundaries. Pyrite occurs as large subhedral to euhedral grains or as aggregates of fine subhedral to euhedral crystals, and commonly contains abundant silicate and sulfide inclusions. Pyrite hosts gold as rounded inclusions within grains, and localized along pyrite grain boundaries.

Table 1: Summary of the geological characteristics of the New Celebration vein system

Deformation Event	Vein Generation	Host Rock	Vein Type	Mineralogy	Width	Structure	Alteration Halo
$D2_{NC}$	Pre-gold veins -Early gold event	Bio-ank mylonites, M1 plg porphyries		qtz, cb	200-1200µ	Foliation parallel deformed quartz boudins	Ankerite?
$D3_{NC}$	Syn-gold veins -early gold event	Bio-cb mylonites, chl schists	Extension	qtz, cb	400-2000µ	Zoned veins, cross-cut by foliation	Ankerite
$D3_{NC}$		Mafic, ultramafic chl-cb schists	Extension	cc	400µ	Thin veins, cross-cut by,foliation	None
$D3_{NC}$		M1 plg porphyry	Shear?	qtz, cc, py,	600-2400µ	Foliation sub-parallel. Biotite edges veins	Ankerite
$D4_{NC}$	Pre-gold veins -Late gold event	M2 fsp-qtz porphyry	Extension - Vein Stockwork	qtz, (cb, ser)	400-4000µ	Buck quartz, forms vein breccia arrays	None
$D4_{NC}$	Syn-gold veins -late gold event	M2 fsp-qtz porphyry	Extension?	ser, chl, py	20-200 µ	Thin fracture veinlets	None

Fluid Inclusion Petrography and Relative Timing Relationships

Fluid Inclusion Petrography

Twelve syn-gold samples representing the four different mineralisation styles were selected from drill core within the New Celebration gold deposits. These samples were prepared as 80µm double-polished thick sections and then petrographically examined for quartz textures and fluid inclusions. Four samples, best representing the different mineralisation styles, were selected for detailed microthermometric analysis. These samples were examined petrographically prior to microthermometric analysis in order to determine the types of inclusions present in the samples and to categorise their morphology, distribution and relative timing. Fluid inclusions in all samples typically ranged in size from <1µm to approximately 30µm and varied in morphology from highly irregular to rounded to negative crystal shaped. Most inclusions selected for microthermometric analysis ranged between 3µm and 15µm in the longest dimension; unusually large or highly irregular inclusions were not analysed as these inclusions are commonly subject to post-entrapment modification. No inclusions suitable for analysis were identified in the Contact style sample.

Detailed petrography of primary, pseudo-secondary and secondary fluid inclusions trapped in Type 2 zoned quartz-carbonate veins in Porphyry- and Mylonite-style mineralisation samples and Type 3 quartz breccia veins in Fracture-style mineralisation revealed four inclusion types: (I) aqueous, (II) aqueous-carbonic, (III) carbonic, and (IV) methane. These inclusion types were further subdivided based on the presence or absence of daughter crystals, behaviour during heating and freezing runs and their composition. Phase ratios of liquid water (L_W), carbonic liquid (L_C) and vapour at room temperature (~22°C) were estimated visually using the volumetric chart of Shepherd et al., (1985). Fluid inclusion composition was

determined using visual and microthermometric means. In the absence of laser Raman analyses the presence of gases such as N_2, H_2S or complex hydrocarbons cannot be quantified.

Type I inclusions are two-phase and liquid-rich at room temperature and comprise H_2O-NaCl±KCl. The volume percent vapour is commonly between 5 and 10%. Type I inclusions are commonly rounded to irregularly shaped, and where they form pseudo-secondary or secondary trails, they are usually elongate in the direction of the trail.

Type II inclusions are mixed H_2O-CO_2-NaCl inclusions, which may contain minor amounts of CH_4 or other gases such as N_2, H_2S or complex hydrocarbons. They are commonly sub-rounded but where they occur in calcite they always have a negative crystal shape. Type II inclusions have been further subdivided depending on whether a discrete carbonic phase is observed. Mixed aqueous-carbonic inclusions at temperatures below the CO_2 critical point (31.1°C) may contain up to 2.2 molal CO_2 without condensing a separate carbonic liquid phase (Ellis and Golding, 1963; Hedenquist and Henley, 1985; Roedder, 1984). Such inclusions appear to be two-phase aqueous inclusions at room temperature but during heating from low temperature, phase transitions at the expected approximate temperature of clathrate melting are observed. Type IIa inclusions represent typical mixed aqueous carbonic inclusions with low to moderate amounts of CO_2. These inclusions may be two or three-phase at room temperature and always contain a carbonic phase. The carbonic phase is commonly pure CO_2 but may contain minor amounts of CH_4 or other gases. The volume of the carbonic phase varies, but typically comprises approximately 40-70% of the inclusion. Some type IIa inclusions contain tiny (<1µm) rounded opaque daughter crystals and rarely may contain larger (up to 5µm) rounded or rod-shaped transparent daughter crystals. Type IIb inclusions are high H_2O- low CO_2, two-phase inclusions which do not nucleate a separate carbonic phase, either at room temperature or at much lower temperatures (-180°C) during freezing experiments.

Type III inclusions are carbonic-only inclusions, but may contain other gases. They may be one- or two-phase at room temperature. Type III inclusions are rare.

Type IV inclusions are methane rich but in the absence of laser Raman analyses cannot be evaluated further. These inclusions are dark, generally rounded, and are always monophase at room temperature. Type IV inclusions are subdivided further based on their mode of occurrence. Type IVa inclusions occur as clusters within the calcite selvedge of zoned quartz-carbonate veins, while, Type IVb inclusions occur as trails in both quartz and calcite. Table 2 summarises the characteristics of each inclusion type.

Table 2: Summary of fluid inclusion types and their chemistry, volume % vapour (aqueous inclusions) or volume % carbonic phase (aqueous-carbonic inclusions) at room temperature, daughter minerals, timing and host vein type. Abbreviations: opq – opaque mineral, dx – daughter crystal; P – primary; PS – pseudo-secondary; S – secondary; qtz – quartz; cc – calcite; bx – breccia.

Inclusion type	Subgroup	Chemistry	Volume% vapour or *carbonic* phase	Other phases	Timing	Vein type	Mineralogy
I	**Ia**	H_2O-NaCl±KCl	5-10		P, PS, S	2 3	Qtz-cc Qtz bx
	Ib	H_2O-NaCl±KCl	5-10		LS	3	Qtz bx
II	**IIa**	H_2O-CO_2-NaCl±CH_4±N_2	*40-70*	Opq dx Clear dx	P, PS	2 3	Qtz-cc Qtz-bx
	IIb	H_2O>>CO_2-NaCl	10-20		PS	3	Qtz-bx
III		CO_2±CH_4±N_2	30-60		P, PS	2 3	Qtz-cc Qtz bx
IV	**IVa**	CH_4±CO_2	0			2	Qtz-cc
	IVb	CH_4	0			2	Qtz-cc

Fluid Inclusion Assemblages and Relative Timing

Fluid inclusions are classified according to the criteria of Roedder (1984) as primary, secondary or pseudo-secondary, according to their location within the host mineral. Primary inclusions occur in clusters, which are randomly distributed in three dimensions within the host crystal and commonly occupy crystal growth zones. They are typically large, relative to the host crystal, and are isolated from their adjacent inclusions. Secondary inclusions define healed fractures and typically occur along planes. They are commonly elongate or irregularly shaped and form trails that crosscut multiple grains. Pseudo-secondary inclusions also define trails in the host mineral, but pseudo-secondary trails terminate at grain boundaries or within individual grains.

Combinations of different inclusion types that occur in clusters or trails and were contemporaneously trapped are commonly referred to as a fluid inclusion assemblage (Diamond, 1990). Crosscutting relationships between the different assemblages and host veins can assist in determining the relative timing of the different inclusion types and fluids. Eight fluid inclusion assemblages are recognized in the syn-gold mineralisation veins at New Celebration. Most assemblages consist of two or more assemblage types but single inclusion type assemblages also occur.

The earliest assemblage observed (assemblage 1) comprises only type IVa methane±carbonic inclusions. These inclusions are primary and occur as clusters in the calcite selvedge of zoned quartz-calcite veins in Porphyry style mineralisation. No direct crosscutting relationships are observed, however their location in the calcite selvedge of the earliest studied vein would suggest that paragenetically they pre-date all other observed inclusion assemblages.

Assemblage 2 is also a mono-inclusion assemblage, and comprises type IIa aqueous-carbonic inclusions. Assemblage 2 is only observed in the carbonate rim of the zoned quartz-calcite veins and shows no crosscutting relationships with assemblage 1. It is unlikely that these assemblages formed contemporaneously; however, their relative timing relationship cannot be determined.

Assemblage 3 comprises type IIa aqueous-carbonic inclusions ± daughter crystals, minor type Ia aqueous inclusions and rare type III inclusions. This assemblage occurs in primary clusters or pseudo-secondary trails in the inner quartz zone of type 2 zoned quartz-calcite veins from Porphyry-style mineralisation.

Assemblage 4 is ubiquitous to all mineralisation styles and comprises only Type Ia aqueous inclusions occurring in secondary trails. In Porphyry-style mineralisation, assemblages 1 to 4 are crosscut by assemblage 5, which is paragenetically the latest assemblage observed. Assemblage 5 comprises secondary trails of Type IVb inclusions.

Assemblage 6 occurs in type 2 zoned quartz-calcite veins from Mylonite-style mineralisation and comprises approximately equal proportions of Type Ia aqueous inclusions and Type III carbonic inclusions, with extremely rare Type IIa aqueous-carbonic inclusions, which occur in pseudo-secondary trails. Assemblage 4 crosscuts assemblage 6.

Assemblage 7 comprises Type Ia aqueous inclusions, types IIa and IIb aqueous-carbonic inclusions and type III carbonic inclusions, which occur in pseudo-secondary trails. This assemblage is crosscut by assemblage 4, which is itself crosscut by Assemblage 8. Assemblage 8 comprises only Type Ib inclusions and is the latest assemblage observed in Fracture-style mineralisation. Table 3 summarises the assemblage types and their relative timing.

Table 3. Summary of assemblages, relative timing, host vein type and mineralisation style. Abbreviations: P – primary; PS – pseudo-secondary; S – secondary; qtz – quartz; cc – calcite; bx –

ASSEMBLAGE	INCLUSION TYPES	TIMING	VEIN TYPE	MINERALISATION STYLE
1	IVa	P	Qtz-cc vein	Porphyry
2	IIa	P	Qtz-cc vein	Porphyry
3	Ia, IIa, III	P, PS	Qtz-cc vein	Porphyry
4	Ia	S	Qtz-cc vein, qtz bx vein	Porphyry, Mylonite, Fracture
5	IVb	S	Qtz-cc vein	Porphyry
6	Ia, III, (IIa)	PS	Qtz-cc vein	Mylonite
7	Ia, IIa, IIb, III	PS	Qtz bx vein	Fracture
8	Ib	S	Qtz bx vein	Fracture

Fluid Inclusion Microthermometry

Analytical Procedure

Microthermometric data were collected using a fully automated Linkham THMSG heating and freezing stage, which has a temperature range of -196° to +600°C. The stage was calibrated against the melting point of pure CO_2 (-56.6) and pure H_2O (0.0°C), and the critical point of pure H_2O (374.1°C) using SynFlinc synthetic fluid inclusion standards. Accuracy of the stage during low-temperature (<32°C) measurements was between ± 0.1° and ±0.4°C and during high temperature measurements (>100°C) was ±4.0°C, while precision was to 0.1°C at all temperatures. Data collected included homogenisation temperature of CH_4 (Th CH_4), melting and homogenisation temperatures of CO_2 (Tm CO_2 and Th CO_2, respectively), eutectic temperature (T_E), ice melting temperature (Tm $_{ICE}$), clathrate melting temperature (Tm $_{CLATH}$), total homogenisation temperature of the inclusion (Th $_{TOT\ (L)}$) and decrepitation temperature (Th $_{DECREP}$). The cycling technique of Goldstein and Reynolds (1994) was employed during heating and freezing experiments in order to obtain accurate phase transition temperatures.

Low Temperature Measurements

In order to observe low temperature phase transitions in all inclusion types, inclusions were first super-cooled to around -50°C for type I inclusions, -110°C for type IIa and type III inclusions and -196°C for type IVa and IVb, then reheated slowly at 1°/minute near expected phase transitions.

Porphyry-style mineralisation: The earliest observed inclusions, Type IVa inclusions, did not freeze above the lower limit of the stage (-196°C). At low temperatures (-100°C) a vapour bubble formed; upon warming these inclusions homogenised to liquid between -76°C and -73°C. In the absence of laser Raman spectroscopy, which would unequivocally determine the gas content of these inclusions, they are interpreted to be CH_4-dominant. Type IVb inclusions also did not freeze upon cooling to -196°C. As for type IVa inclusions, a vapour bubble formed at low temperatures, but in contrast to the earlier inclusions homogenised to liquid at around -90°C. These inclusions may also contain a gas phase other than CH_4; however, this cannot be determined without further analysis using other techniques.

The majority of type IIa inclusions displayed CO_2 melting temperatures at or only marginally below the CO_2 triple point (-56.6°C), indicating that the CO_2 phase of these inclusions was pure, or only contained trace proportions of other gases. Type IIa inclusions in calcite showed the least variation in Tm CO_2, between -56.6° and -56.7°C, suggesting a total absence of other gases, while the majority of the quartz-hosted Type IIa inclusions ranged between -56.6° and 58.7°C with outliers of up to -61.0°C (Figure 1). Clathrate melting temperatures for the calcite-hosted inclusions ranged from 8.4° to 9.6°C while the quartz-hosted inclusions showed a slightly broader range from 6.0° to 8.6°C (Figure 1). At higher temperatures, CO_2 homogenised to liquid at temperatures between 28.9° and 30.8°C in calcite-hosted inclusions and between 6.5° and 30.5°C in quartz-hosted inclusions (Figure 1).

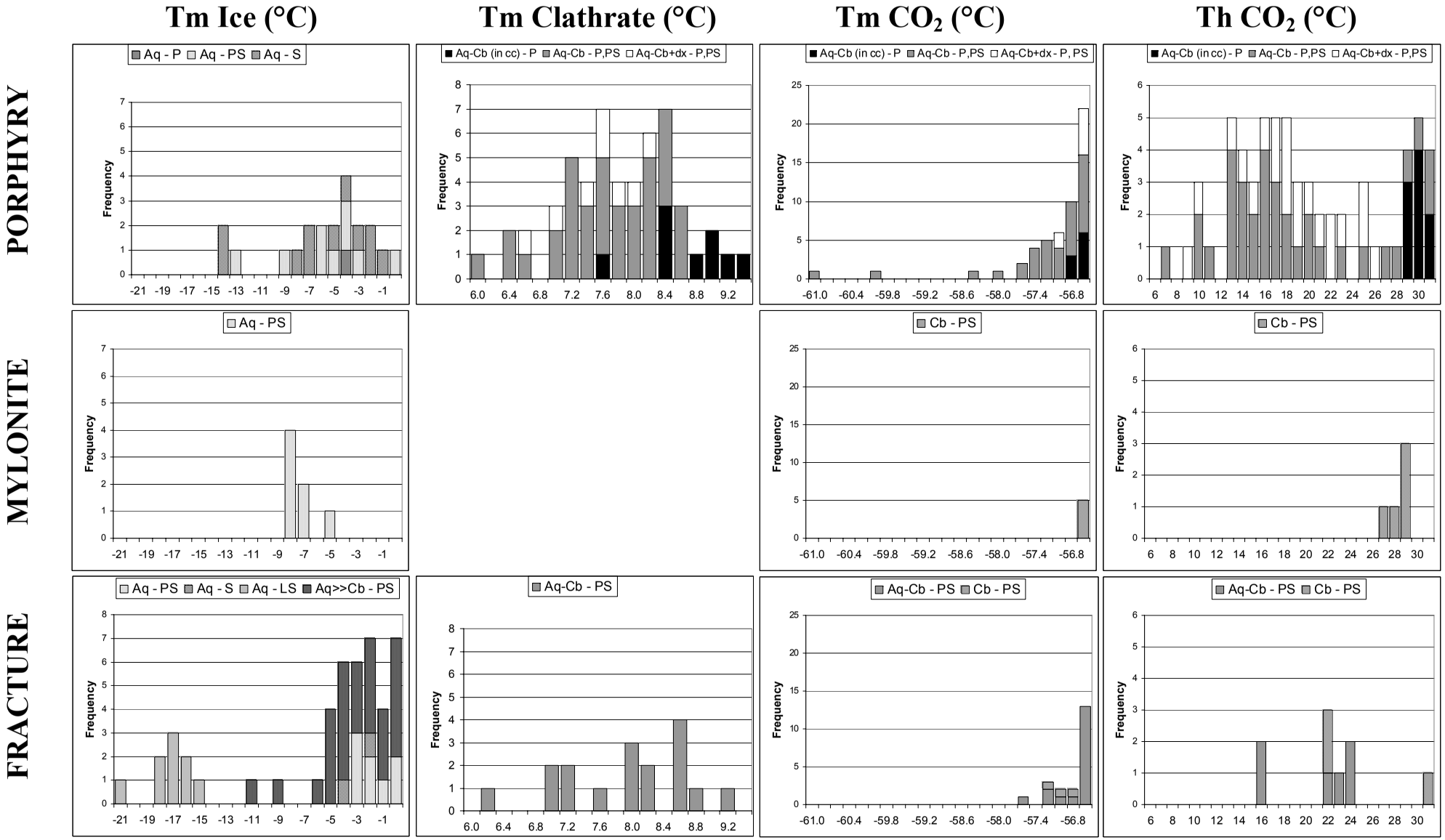

Figure 1: Histograms of final ice-melting temperature (Tm $_{ICE}$), clathrate melting temperature (Tm $_{CLATH}$) CO_2 melting temperature (Tm CO_2), CO_2 melting temperature (Tm CO_2) and CO_2 homogenisation temperature (Th $CO_{2\,(L)}$, from primary (P), pseudo-secondary (PS), secondary (S) and late secondary (LS) aqueous (Aq), aqueous-carbonic and carbonic (Cb) inclusions in Type 2 zoned quartz-calcite veins from Porphyry- and Mylonite- styles of mineralisation and Type 3 quartz breccia veins from Fracture-style mineralisation. All inclusionsare hosted in quartz except where indicated in the legend.

In Type I aqueous inclusions the initial ice-melting temperature, or eutectic temperature, was difficult to observe due to their small size (<10μm). Where the eutectic temperature was observed, it occurred at approximately -24°-20°C, indicating that the inclusions are likely within the H_2O-NaCl±KCl system (Shepherd et al., 1985). Final ice melting temperatures showed a wide range from -10° to 0.0°C with the majority of inclusions showing final ice melting temperatures at around -2.0° to -6.0°C (Figure 1).

Mylonite-style mineralisation: Type I aqueous inclusions also showed eutectic temperatures ranging between -24° and -20°C, while final ice melting temperatures ranged from -8° to -4 °C.

Type III carbonic inclusions all melted at -56.6°C, indicating they were composed of pure CO_2, and homogenised to liquid at temperatures between 28° and 30°C (Figure 1).

Fracture-style mineralisation: Final ice melting temperatures of Type I aqueous inclusions in Fracture-style mineralisation delineated two populations: 1) a high temperature population that showed final ice-melting temperatures between -5° and 0°C (Type Ia), and 2) a lower-temperature group, which showed final ice-melting temperatures between -15° and -22° (Type Ib) (Figure 1). As for previous mineralisation styles, eutectic temperatures indicated that these inclusions belonged to the H_2O-NaCl-KCl system.

The CO_2 melting temperature of Type IIa inclusions clustered tightly around -56.6 °C, with a minimum temperature of -57.3°C, indicating other gas phases such as CH_4 are rare or absent. Clathrate melting temperatures range between 6.2° and 9.2°C. The CO_2 phase homogenised to liquid at temperatures between 16° and 24°C (Figure 1).

Type IIb inclusions did not contain enough CO_2 to condense a separate phase, therefore, the phase-transitions usually observed in mixed aqueous-carbonic inclusions were not seen. At low temperatures, these inclusions behaved like two-phase aqueous inclusions, freezing at around -60°C and final ice melting between -7° and 0°C. These inclusions however, also showed a phase transition around 6.0 to 9.0°C, which is the temperature range expected for clathrate melting in typical mixed H_2O-CO_2 inclusions.

Rare type III carbonic inclusions melted finally at between -57.4°C and -56.8°C and homogenised into liquid at temperatures ranging from 21°C to 31°C (Figure 1).

High Temperature Measurements

Heating experiments were conducted on representative inclusions from the different mineralisation styles. The best chips from each style were excluded from heating experiments as high temperatures may destroy fluid inclusions rendering them useless for other analytical methods such as laser Raman spectroscopy or laser ablation – inductively coupled plasma mass spectroscopy (LA-ICPMS). The chips were heated at 5°C/minute below 200°C and 1°C/minute above 200°C, and measurements were obtained in sequence from liquid-rich to vapour-rich inclusions in order to avoid destroying high-pressure inclusions prior to obtaining homogenisation temperatures.

Porphyry-style mineralisation: Homogenisation data for Type Ia aqueous inclusions are sparse and poorly constrained as these inclusion types are rare in Porphyry style mineralisation. Type Ia inclusions homogenised to liquid at temperatures ranging between 180°C and 360°C, although most clustered between 240°C and 280°C.

Type IIa inclusions in calcite were tightly constrained and either homogenised to liquid or homogenised via expansion of the vapour bubble prior to decrepitation between 267°C and 271°C. Type IIa inclusions in quartz showed a much wider temperature distribution. Homogenisation (to liquid) or decrepitation (via vapour bubble expansion) occurred at between 220°C and 290°C for the majority of these inclusions although rare inclusions homogenised to liquid at about 360°C.

Mylonite-style mineralisation: Type Ia inclusions in the Mylonite style sample homogenised at slightly lower temperatures when compared to Porphyry-style. These inclusions also showed considerable spread in the data and homogenised to liquid at temperatures between 120°C and 220°C.

Fracture-style mineralisation: Type Ib aqueous inclusions are unique to Fracture-style mineralisation and are quite different from other aqueous inclusions observed in the earlier mineralisation event. These inclusions homogenised to liquid at very low temperatures, between 87°C and 102°C. Like Type IIa inclusions in the Porphyry style sample, rare Type IIa inclusions either homogenised to liquid or decrepitated to vapour over a wide temperature range between 180°C and 360°C. Type IIb inclusions

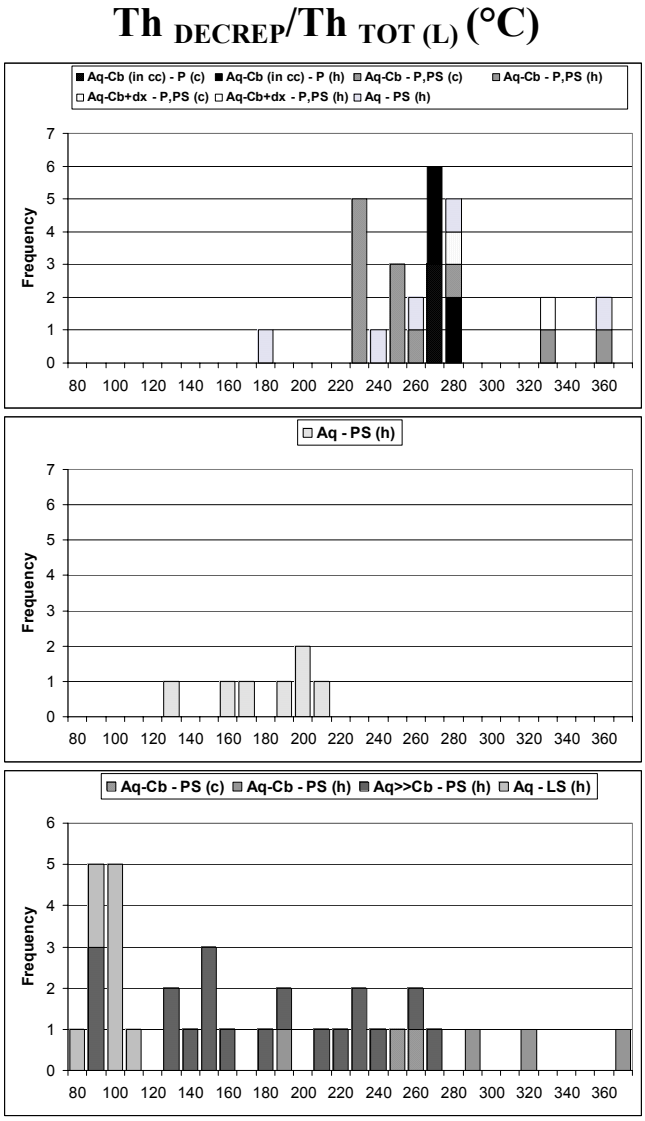

Figure 2: Histograms of decrepitation temperature (Th $_{DECREP}$) and homogenisation temperature of primary (P), pseudo-secondary (PS), secondary (S) and late secondary (LS) aqueous (Aq), aqueous-carbonic and carbonic (Cb) inclusions in Type 2 zoned quartz-calcite veins from Porphyry- and Mylonite- styles of mineralisation and Type 3 quartz breccia veins from Fracture-style mineralisation. All inclusionsare hosted in quartz except where indicated in the legend.

homogenised to liquid at temperatures between 120°C and 270° C, with rare inclusions homogenising at temperatures closer to 80°C.

Quantitative Composition of Fluid Inclusions

Salinity (equiv. wt% NaCl), bulk composition and density were calculated using MacFlinCor (Brown and Hagemann, 1995) and the equations of state for H_2O-NaCl-KCl (Bodnar and Vityk, 1994), and H_2O-CO_2-CH_4-NaCl and CO_2-CH_4 (Jacobs and Kerrick, 1981). The graphical methods of Swanenberg (1979) and Thiery et al. (1994) were used to estimate the molar proportions of CO_2 and CH_4. The following data summarise the results of the heating experiments and are also presented graphically in Figure x. Salinity is reported in equivalent weight % NaCl, except for type IIb inclusions for which the apparent salinity is reported (see below). The relative proportions of CO_2 and CH_4 are reported in mole fractions (X) and density is reported in grams per cubic centimetre (g/cm^3).

Fluid composition and density

Salinity in fluid inclusions is typically expressed as equivalent weight percent NaCl and specifically refers to the total dissolved solids in a solution (e.g. Chou, 1964). In aqueous inclusions salinity is determined using final ice melting temperatures (Bodnar, 1993; Roedder, 1963), while in mixed aqueous-carbonic inclusions final clathrate melting temperatures are used to assess the salinity (Collins, 1979). In mixed inclusions that do not contain enough CO_2 to condense a separate phase, CO_2 acts as a simple dissolved species and at CO2 pressures between 10.4 and 0 bars will depress the final ice melting temperature of pure water by -1.5°C (Hedenquist and Henley, 1985). This means that the estimated salinity obtained from ice melting temperatures of such mixed inclusions will be too low. Clathrate melting temperatures were obtained from most type IIb apparently aqueous inclusions, however, where clathrate melts in the absence of liquid CO_2, the salinity calculation is not valid (Diamond, 1992). As there is no method to calculate the effect of CO_2 on fluids which contain more than about 0.5 equivalent weight percent NaCl (Hedenquist and Henley, 1985), the salinity of type IIb inclusions is reported as apparent salinity and reflects the maximum salinity of these inclusions; the true value is probably lower.

Porphyry style mineralisation: The salinity of Type Ia aqueous inclusions is variable and ranges between 1 and 18 equiv. wt % NaCl (Fig. 3). The majority of data from primary, pseudo-secondary and secondary

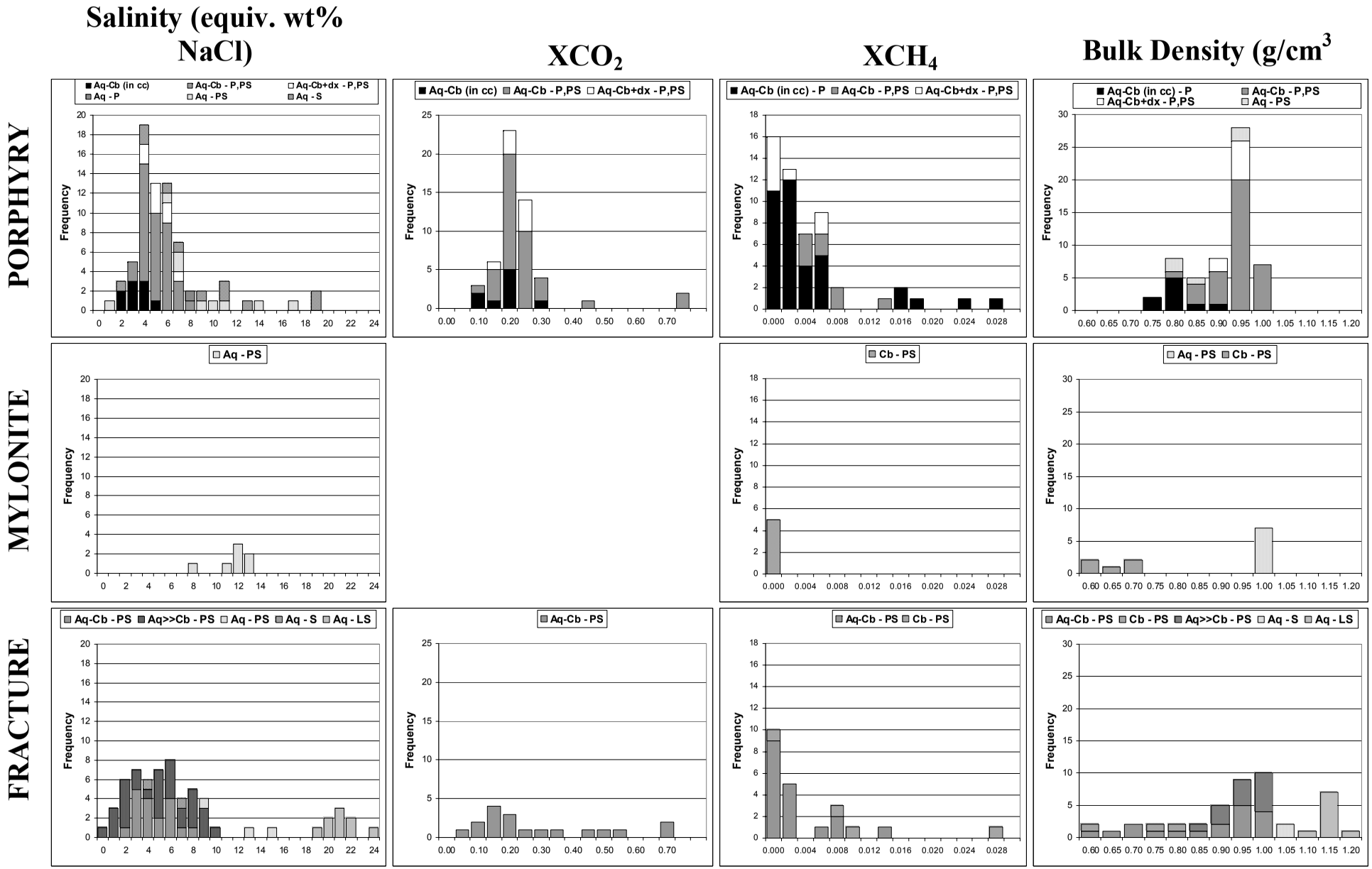

Figure 3: Histograms of salinity (equivalent wt% NaCl), molar proportions of CO_2 (XCO_2) and CH_4 (XCH_4) and bulk density from primary (P), pseudo-secondary (PS), secondary (S) and late secondary (LS) aqueous (Aq), aqueous-carbonic and carbonic (Cb) inclusions in Type 2 zoned quartz-calcite veins from Porphyry- and Mylonite- styles of mineralisation and Type 3 quartz breccia veins from Fracture-style mineralisation. All inclusions are hosted in quartz except where indicated in the legend.

inclusions cluster between 5 and 11 equiv. wt% NaCl and the different inclusion types cannot be separated on the basis of their salinity. The data from type IIa inclusions are more tightly constrained; Type IIa inclusions in calcite have salinities which range from 1 to 5 equiv. wt.% NaCl, while the salinity of Type IIa inclusions in quartz ranges from 3 to 9 equiv. wt% NaCl. The molar proportion (X) of CO_2 was relatively low in type IIa inclusions from both quartz and calcite and ranged between 0.1 and 0.3 although rare inclusions in quartz contained up to 0.8 XCO_2. The XCH_4 was generally very low (Figure 4) in all Type IIa inclusions and ranged from 0.0 to 0.03. The bulk density of all inclusions ranged from 0.75 to 1.05 g/cm3. Type IIa inclusions in calcite were less dense than all other inclusions within the same sample.

Mylonite-style mineralisation: Type Ia inclusions have similar salinities and densities to those in Porphyry-style mineralisation. Type III inclusions are pure CO_2 (i.e. they contain no CH_4) and have densities ranging between 0.60 and 0.70 g/cm3.

Fracture-style mineralisation: The salinity of Types Ia, IIa and IIb inclusions range from 0 to 15wt%, which is within the range of similar inclusions in porphyry and Mylonite styles of mineralisation. Type Ib inclusions however, are much more saline and range between 19 and 23 equiv. wt% NaCl. These inclusions are also the densest of all inclusions observed, with densities around 1.10 to 1.20 g/cm3. The XCO_2 and XCH_4 of type IIa inclusions displayed more variability than those in Porphyry-style mineralisation, and ranged from 0.10 to 0.70 and 0.00 to 0.03 respectively. The bulk density of these inclusions was also very variable and ranged from 0.60 to 1.05 g/cm3.

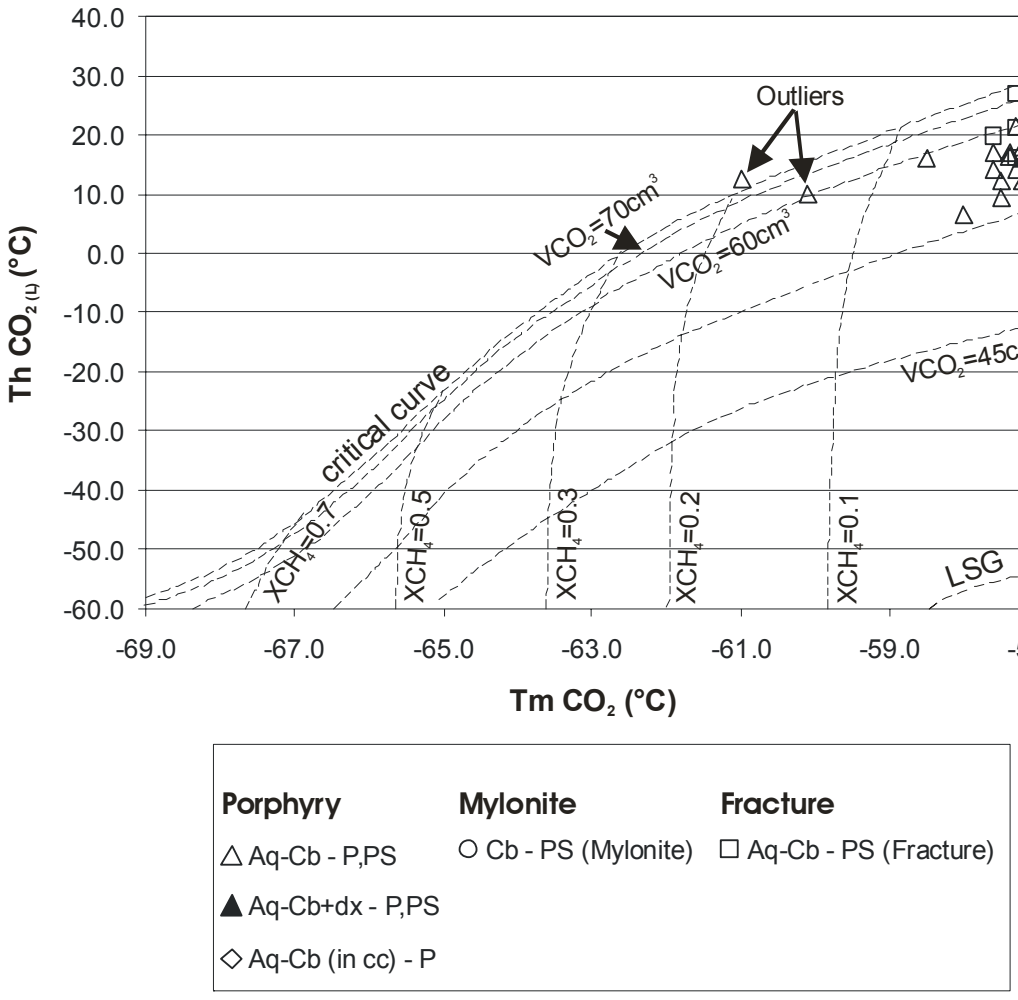

Figure 4: CO_2 melting temperature (Tm CO_2) versus CO_2 homogenisation temperature (Th $CO_{2\ (L)}$) of carbonic and aqueous-carbonic (±daughter crystals) inclusions in Type 2 zoned quartz-calcite veins from Porphyry- and Mylonite styles of mineralisation and Type 3 quartz breccia veins from Fracture-style mineralisation. Inclusions cluster tightly and indicate that the fluids trapped during Porphyry-, Mylonite and Fracture styles of mineralisation were low in CH_4 (<10 mol%). The outliers may reflect a separate population under-represented in the current data set. Conversely, increased data may highlight a continuum from low CH_4 to higher CH_4 and increasing density

Geological Processes

Fluid Immiscibility

Fluid immiscibility is a commonly invoked mechanism for hydrothermal ore deposit formation (Wilkinson, 2001), however, recognising phase separation from fluid inclusions in a hydrothermal system

is not simple. Fluid inclusions in the CO_2-H_2O system can only have been trapped in one of two P-T states. Either they were trapped from a homogeneous fluid in the single phase field, or they were trapped from a heterogeneous fluid in the two-phase field (Diamond, 2001). In theory, the state of entrapment of cogenetically trapped inclusions should be readily distinguishable by applying the principle of uniformity of phase volume proportions (Roedder, 1984; Sorby, 1858). Inclusions trapped contemporaneously in the single phase field should have similar compositions, bulk molar volumes and phase proportions. Conversely, inclusions trapped in the two phase field will show highly variable bulk compositions, bulk molar volumes and phase proportions (Diamond, 2001; Loucks, 2000).

Within individual assemblages, Type IIa inclusions in Porphyry-style mineralisation show very little variation of phase proportions, bulk composition or molar volume. Inclusions within individual assemblages do not display liquid-rich and vapour-rich end-members, suggesting that phase separation has not occurred (c.f. Diamond, 2001).

Phase proportions, bulk compositions and molar volumes of Type IIa inclusions in assemblage 7 of Fracture-style mineralisation show more diversity within a single cluster or trail than those in the Porphyry style assemblages and may be the consequence of fluid immiscibility. In situations where both liquid-rich and vapour-rich fluid inclusions occur in a cogenetic assemblage, Ramboz et al. (1982) have outlined three criteria to determine whether phase separation has taken place. These are:

1. *"The two types of inclusions must occur in the same regions of the same sample, and there must be good evidence for their contemporaneous trapping".* Type IIa inclusions in the Fracture-style samples consistently occurred in pseudo-secondary trails with Type IIb mixed inclusions in assemblage 7. The different inclusion types occurred in similar ratios in all observed trails. The consistency of these relationships in a number of occurrences is evidence that these inclusion trails were trapped contemporaneously and that the inclusions represent a cogenetic assemblage.
2. *"The two types of inclusions must homogenise at the same temperature, or more realistically within the same range of temperature (because trapping is not an instantaneous and strictly isothermal-isobaric process). One type must homogenise into a liquid (V + L→L), the other must homogenise into a vapour (V + L→V).* Type IIa and IIb inclusions in Fracture style mineralisation did not satisfy this criterion. Inclusions showed a wide range of homogenisation temperatures, from 120° to 280°C, with rare higher temperature outliers. Further, all inclusions homogenised to liquid.
3. *"Upon heating, the pressures in the two types of inclusions before homogenisation are different (because of the difference in their compositions and densities). The pressures reach the same value (trapping pressure) at homogenisation temperature. Therefore, if one inclusion type decrepitates before homogenising, the other type must behave similarly."* This criterion could not be evaluated as, except for two inclusions, all inclusions homogenised and did not decrepitate.

To further evaluate the possibility of fluid immiscibility in veins from the New Celebration gold deposit, inclusions from Porphyry and Fracture styles of mineralisation were plotted on a ternary H_2O-CO_2-NaCl diagram (Figure 5), including the solvi for 300°C and 500°C at 1.5kbar from Pichavant et al. (1982). Inclusions from both mineralisation styles plotted below the 300°C solvus in the single phase field, indicating that it is unlikely phase separation took place during either mineralising event. There are currently no published solvi for low temperature (300° to 500°C) and moderate to high pressure (3-4kbar) however increasing the pressure of the system pushes the solvus up towards the centre of the triangle, thereby increasing the single phase field, therefore, the interpretation of these data would not change even with a higher temperature solvus.

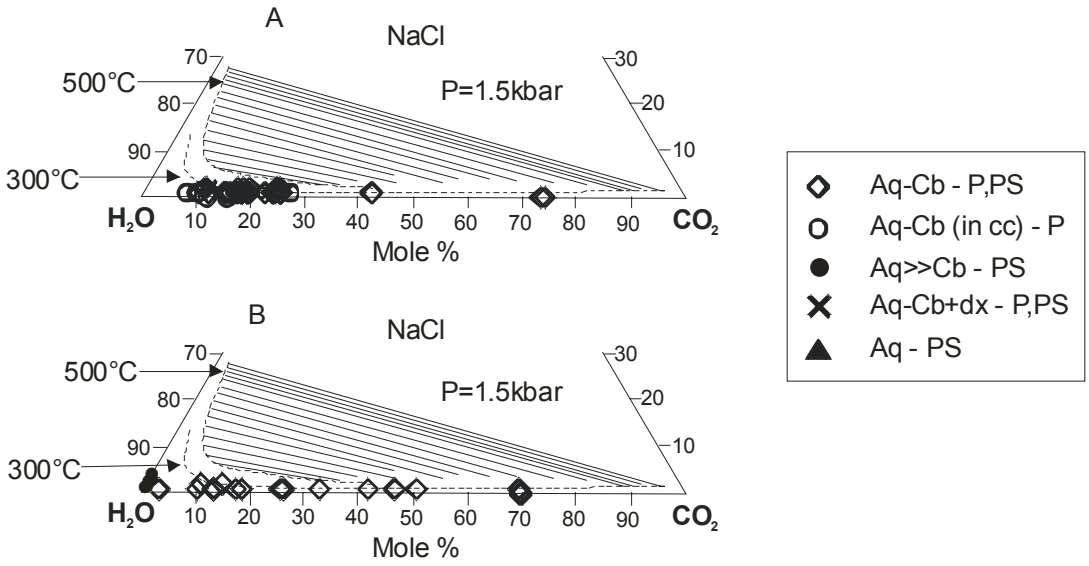

Figure 5: Ternary diagram of coexisting aqueous (Aq) and aqueous-carbonic primary (P) and pseudo-secondary (PS) inclusion from Porphyry (A) and Fracture (B) mineralisation styles with the solvi for the system H_2O-CO_2-NaCl at 1.5kbar, 300° and 500°C. Tie lines link liquid and vapour fields. Solvi and tie lines from Pichavant et al. (1982). All inclusions from both mineralisation styles are located below the 300°C solvus in the single phase field and there are no boiling pairs joined by tie lines. There is no evidence from the current data set the phase separation took place during either mineralising event. There are no available experimental data for the H_2O-CO_2-NaCl system at temperatures between 300° and 500°C and pressures upwards of 3kbar, however, increasing pressure drives the solvus upwards and away from the base of the triangle thereby increasing the size of the single phase field.

Fluid mixing

Fluid mixing is also an excellent mechanism for ore deposition (Wilkinson, 2001). A bivariate plot of homogenisation temperature (Th $_{TOT}$) versus salinity (equiv. wt% NaCl) should indicate a linear relationship between end-member fluids if mixing has taken place. Figure 6 plots these parameters for the different mineralisation types at New Celebration, but no clear trends can be elucidated from the current data set. Further data are required in order to adequately assess the possibility of fluid mixing

PORPHYRY **MYLONITE** **FRACTURE**

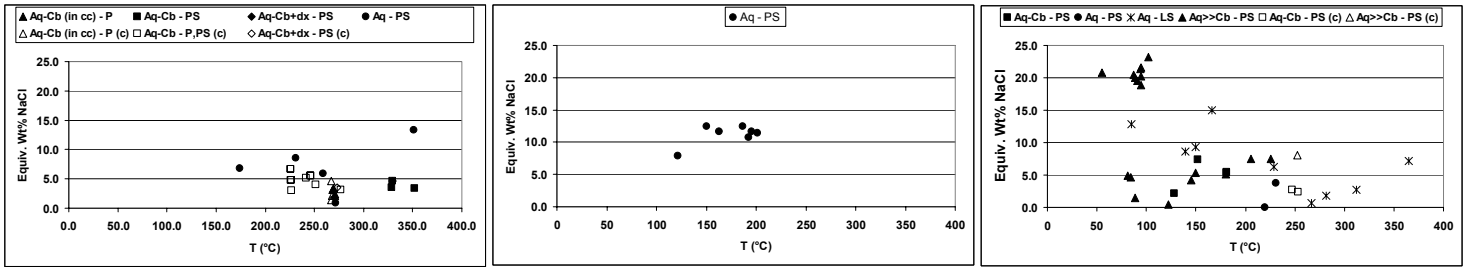

Figure 6: Decrepitation temperature (Th $_{DECREP}$) or homogenisation temperature (Th $_{TOT\ (L)}$) versus salinity (equivalent weight % NaCl) for primary (P), pseudo-secondary (PS), secondary (S) and late secondary (LS) aqueous (Aq) and aqueous-carbonic (Aq-Cb) fluid inclusions from Type 2 zoned quartz-calcite veins from Porphyry and Mylonite styles of mineralization and Type 3 quartz breccia veins from Fracture style mineralization. The data set is currently too limited to evaluate the possibility of fluid mixing.

Implications for gold mineralisation

As there is insufficient evidence for either phase separation or fluid mixing at New Celebration, some other method by which gold mineralisation occurred must be employed. In all mineralisation styles, gold is hosted within pyrite, and gold enrichment shows a close correlation with increasing pyrite (Nichols, 2003; Williams, 1994). Williams (1994) and Nichols (2003) both report a strong lithological control on gold grade. The gold-related fluid is low-salinity; therefore, it is unlikely gold was transported in a chloride complex. The most likely scenario is that gold was transported as a bisulfide complex and was precipitated by desulfidation reactions due to interaction with iron-rich wall rocks. This correlates with the mechanism that Williams (1994) proposed for the formation of the Southern Ore Zone. The current data do not support fluid unmixing as a mechanism by which gold mineralisation took place at New Celebration, however, the data from Fracture-style mineralisation are equivocal. Further data are required to confirm whether phase separation played a role in gold mineralisation at New Celebration.

P-T-t History of Hydrothermal Fluids

Trapping Temperatures

Except where fluid immiscibility is clearly demonstrated, homogenisation temperatures of fluid inclusions do not represent trapping temperatures. As fluid inclusions cannot homogenise at temperatures below those in which they were trapped, homogenisation temperatures represent the minimum formation temperature. Independent pressure estimates are required in order to recalculate the true trapping temperature of aqueous inclusions (Potter, 1977) or estimate formation conditions of aqueous-carbonic inclusions from isochors. Figure 7 shows representative isochors of inclusion types from both Early and Late mineralisation styles, as well as the independent pressure estimate of Williams (1994) and the likely pressure constraints determined from this study. Interpretation of the microthermometric data indicate that the earliest observed aqueous-carbonic inclusions in calcite formed at around 3-4kbar from a hot fluid between 550° and 650°C. Porphyry-style mineralisation formed at similar pressures from a cooler fluid, between 360° and 450°C, while Mylonite-style mineralisation formed between 330° and 360°. Fracture style mineralisation formed at the same pressure as Early mineralisation and at temperatures between 290° and 350°. Fluid inclusion geothermobarometry on representative quartz and quartz-calcite veins from the different mineralisation styles suggests isobaric cooling during both Early and Late mineralising events

Preliminary Hydrothermal Model

The following section presents a preliminary hydrothermal model for hydrothermal fluid flow and associated gold mineralisation during $D3_{NC}$ and $D4_{NC}$ deformation events, based on observations and interpretations of the mineralising vein system, fluid inclusion data and the previous work of Nichols (2003) on the structural setting and hydrothermal alteration of the New Celebration gold deposits.

- The earliest observed $CH_4 \pm CO_2$ fluid inclusions possibly represent a background, regional-scale fault-zone fluid. The source of this fluid is unknown; it may be mantle derived or could be a deep-crustal metamorphic fluid.
- At or near peak metamorphic conditions the fault experienced a localised pulse of hot fluid of unknown origin (possibly magmatic?) which formed early aqueous-carbonic inclusions in calcite. As this fluid cooled at approximately constant pressure it interacted with iron-rich wall rocks, which triggered the Early mineralising event, precipitating Porphyry and Mylonite (and possibly Contact?) style gold due to desulfidation reactions.
- A later aqueous fluid event overprinted Early mineralisation.
- At post-peak metamorphic conditions (late D3 or early D4?), a second, localised burst of fluid, slightly cooler than the first, ascended along the fault. This fluid was responsible for the second, Late mineralising event
- This was followed by a cool dense brine, which formed the late secondary, highly saline inclusions.
- As the localised mineralising fluids dissipated, the fault returned to steady state with background, regional scale methane-dominated fluids returning.

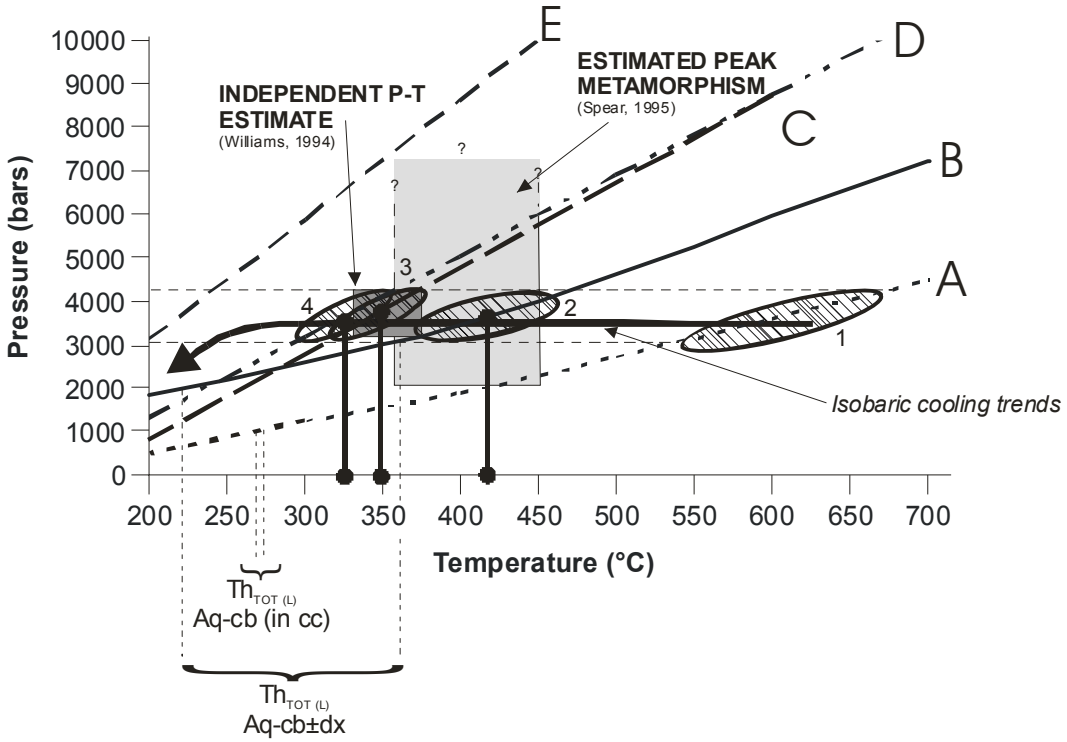

Figure 7: P-T-t diagram showing representative isochores for primary aqueous-carbonic inclusions in calcite (A - Porphyry style mineralisation), primary and pseudo-secondary aqueous-carbonic inclusions± daughter crystals (B - Porphyry and Fracture style mineralisation), pseudo-secondary aqueous inclusions (C - Mylonite style mineralisation) pseudo-secondary aqueous>>carbonic inclusions (D - Fracture style mineralisation) and late secondary aqueous inclusions (E - Fracture style mineralisation). Also shown are the range of homogenization temperatures of primary aqueous-carbonic inclusions in calcite and primary and pseudo-secondary±daughter crystals inclusions represented by isochores A and B, respectively. Assuming isobaric conditions the maximum homogenisation temperature of primary and pseudo-secondary aqueous-carbonic inclusions, represented by isochore B, constrains the minimum trapping pressure of these inclusions to approximately three kilobars. An independent P-T estimate for the Southern Ore Zone mineralization at New Celebration derived from the chlorite solid-solution geothermometer and phengite geobarometer provides an upper pressure constraint of 4.2 kilobars (Williams, 1994). The hatched ovals represent the likely trapping temperatures for each inclusion type at pressures between 3 and 4 kilobars, and correspond well with pressure corrected (i.e. temperature corrected) homogenisation temperatures of cogenetic aqueous inclusions, which constrain the true trapping conditions (c.f. Potter, 1977). Trapping temperatures are shown by heavy lines with filled circles at each end. Isochores from both Early (A to C) and Late (B, D and E) mineralisation events show a cooling trend at constant pressure. Porphyry-style gold mineralization likely occurred at temperatures between 360°C and 450°C and at pressures between 3 and 4 kilobars (hatched oval 2), while Mylonite-style mineralisation occurred at around 330-360°C at similar pressures (hatched oval 3) from a hydrothermal fluid that cooled from temperatures initially as high as 550-650°C (hatched oval 1). It is interesting to note that the likely P-T conditions for Mylonite-style mineralisation correspond almost exactly with the independent P-T estimate for the Southern Ore Zone mineralisation of Williams (1994). The Late mineralising event, represented by isochores B and D from Fracture style mineralisation occurred at similar temperatures and pressures (hatched oval 4) to the Early mineralising event and also followed an isobaric cooling path. This event was probably the result of a second pulse of hydrothermal fluid introduced into the system. The representative isochore for late secondary aqueous inclusions (E) shows a P-T relationship outside of the range for gold mineralization, indicating that these inclusions are unlikely to be gold related.

Conclusions

Interpretation of the vein system and detailed petrography of the fluid inclusion assemblages associated with gold mineralisation at the New Celebration gold deposit leads to the following preliminary conclusions:

1) Four major vein groups that are correlated with specific deformation events and gold mineralisation styles, were identified at New Celebration and a paragenetic sequence was developed: 1) pre-early gold qtz-cc "boudin" veins developed prior to $D3_{NC}$; 2) syn-early gold quartz, calcite or quartz-calcite veins developed during $D3_{NC}$; 3) pre-late gold quartz breccia

veins developed syn-late $D3_{NC}$ or post $D3_{NC}$; and 4) syn-late gold sericite-chlorite-pyrite veins possibly developed during $D4_{NC}$

2) Inclusions were classified according to their occurrence relative to the host grain or grains into primary, pseudo-secondary or secondary.
3) Detailed fluid inclusion petrography on representative vein samples from Porphyry-, Mylonite- and Fracture-style mineralisation revealed four main fluid inclusion types:
    - H_2O-NaCl±KCl inclusions with two sub-populations: low- to moderate-salinity (0-12 equiv. wt% NaCl), and high-salinity (18-22 equiv. wt% NaCl)
    - H_2O-CO_2-NaCl±CH_4±daughter crystals inclusions with a sub-population which appeared aqueous but that contained between 0 and 2.2 molal CO_2
    - CO_2±CH_4±N_2 inclusions, and
    - CH_4±CO_2 inclusions
4) Eight assemblages comprising single inclusions or combinations of inclusions were identified and characterised according to their relative timing and the mineralisation style in which they occurred. The earliest assemblage in Porphyry-style mineralisation comprised primary CH_4±CO_2 inclusions and was crosscut by the mineralising assemblages, which were observed in all mineralisation styles, and which comprised aqueous-carbonic±aqueous±carbonic±aqueous>>carbonic inclusions. The mineralising assemblages were themselves crosscut by low-salinity aqueous inclusions, which were also observed in all mineralisation styles, and which were crosscut by later high-salinity aqueous inclusions in Fracture-style mineralisation. The latest observed assemblage comprised late secondary CH_4 inclusions. This assemblage was only observed in Porphyry-style mineralisation.
5) Type 2 zoned quartz-calcite veins associated with $D3_{NC}$ deformation and Porphyry- and Mylonite-styles of gold mineralisation formed from H_2O-CO_2-NaCl-dominated fluids with salinities between 1 and 8 equiv. wt% NaCl, which contained between 10 and 30 mole % CO_2 and little or no CH_4.
6) Type 3 quartz breccia veins associated with $D4_{NC}$ deformation and Fracture-style mineralisation formed from H_2O-CO_2-NaCl-dominated fluids with salinities between 0 and 12 equiv. wt% NaCl, which contained between 10 and 60 mole% CO_2 and trace (<1 mole %) CH_4
7) The lack of evidence for either fluid immiscibility or fluid mixing, and the low salinity of the ore-related fluids, in combination with the direct correlation between gold grade and pyrite abundance, and the lack of free gold in any mineralisation style, suggested that gold precipitation by wall-rock interaction and desulfidation reactions were the likely mechanism for gold formation at the New Celebration gold deposits.
8) Porphyry-style mineralisation took place at temperatures between 360 and 450°C and between 3 and 4kbar. Mylonite style mineralisation occurred between 330 and 360°C at similar pressures.
9) Fracture-style mineralisation occurred at around 300 and 350°C and between 3 and 4kbar from a second pulse of hydrothermal fluid.
10) Combined geothermobarometry on representative quartz and quartz-calcite veins from Porphyry, Mylonite and Fracture styles of mineralisation suggests an isobaric cooling history during Early and Late stages of gold mineralisation.
11) The mineralising fluids were post-dated by late-stage saline brines and hydrocarbon fluids, both of which were unrelated to mineralisation. The hydrocarbon fluids likely represent the background regional fault zone fluids.

References

Bateman, R. J., Hagemann, S. G., McCuaig, T. C., and Swager, C., 2001, Protracted gold mineralisation throughout Archaean orogenesis in the Kalgoorlie camp, Yilgarn Craton, Western Australia: structural, mineralogical and geochemical evolution, *in* Hagemann, S. G., Neumayr, P., and Witt, W. K., eds., World-class Gold Camps and Deposits in the Eastern Yilgarn Craton, Western Australia, with Special Emphasis on the Eastern Goldfields Province, Record 2001/17, Western Australian Geological Survey, p. 63-98.

Binns, R. A., Gunthorpe, R. J., and Groves, D. I., 1976, Metamorphic patterns and development of greenstone belts in the Eastern Yilgarn Block, Western Australia, *in* Windley, B. F., ed., The early history of the earth: London, Wiley, p. 303-313.

Bodnar, R. J., 1993, Revised equation and table for determining the freezing point depression of H_2O-NaCl solutions: Geochimica et Cosmochimica Acta, v. 57, p. 683-684.
Bodnar, R. J., and Vityk, M. O., 1994, Interpretation of microthermometric data for H_2O-NaCl inclusions, *in* De Vivo, B., and Frezzotti, M. L., eds., Fluid Inclusions in Minerals: Methods and Applications, Virginia Polytechnic Institute Press, p. 117-130.
Brown, P. E., and Hagemann, S. E., 1995, MacFlinCor and its application to fluids in Archean lode-gold deposits: Geochimica et Cosmochimica Acta, v. 59, p. 3943-3952.
Chou, V. T., 1964, Oceanography, *in* Chou, V. T., ed., Handbook of applied hydrology: New York, McGraw Hill.
Collins, P. L. F., 1979, Gas hydrates in CO_2-bearing fluid inclusions and the use of freezing for estimation of salinity: Economic Geology, v. 74, p. 1435-1444.
Diamond, L. W., 1990, Fluid inclusion evidence for P-V-T-X evolution of hydrothermal solutions in late alpine gold-quartz veins at Brusson, Val d'ayas, Northwest Italian Alps: American Journal of Science, v. 290, p. 912-958.
Diamond, L. W., 1992, Stability of clathrate hydrate + CO_2 liquid + CO_2 vapour + aqueous KCl-NaCl solutions: Experimental determination and application to salinity estimates of fluid inclusions: Geochimica et Cosmochimica Acta, v. 56.
Diamond, L. W., 2001, Review of the systematics of CO_2-H_2O fluid inclusions: Lithos, v. 55, p. 69-99.
Dielemans, P., 2000, Structural controls on gold mineralisation in the Southern Ore Zone of the Hampton-Boulder deposit, New Celebration gold mine, Western Australia: Unpub. MSc. thesis, University of Western Australia, 185 p.
Eisenlohr, B. N., Groves, D. I., and Partington, G. A., 1989, Crustal scale shear zones and their significance to Archaean gold mineralisation in Western Australia: Mineralium Deposita, v. 24, p. 1-8.
Ellis, A. J., and Golding, R. M., 1963, The solubility of carbon dioxide above 100°C in water and in sodium chloride solutions: American Journal of Science, v. 261, p. 47-60.
Goldstein, R. M., and Reynolds, T. J., 1994, Systematics of fluid inclusions in diagenetic minerals. SEPM Short Course, 31 p.
Groves, D. I., Barley, M. E., and Ho, S. E., 1990, Nature, genesis and tectonic setting of mesothermal gold mineralisation in the Yilgarn Block, Western Australia: Economic Geology Monograph, v. 6, p. 71-85.
Hedenquist, J. W., and Henley, R. W., 1985, The importance of CO_2 on freezing point measurements of fluid inclusions: evidence from active geothermal systems and implications for epithermal ore deposition: Economic Geology, v. 80, p. 1379-1406.
Jacobs, G. K., and Kerrick, D. M., 1981, Methane: An equation of state with application to the ternary system H_2O-CO_2-CH_4: Geochimica et Cosmochimica Acta, v. 45, p. 607-614.
Loucks, R. R., 2000, Precise geothermometry on fluid inclusion populations that trapped mixtures of immiscible fluids.: American Journal of Science, v. 300, p. 23-59.
Mueller, A. G., Harris, L. B., and Lungan, A., 1988, Structural control of greenstone-hosted gold mineralisation by transcurrent shearing: a new interpretation of the Kalgoorlie Mining District, Western Australia: Ore Geology Reviews, v. 3, p. 359-387.
Neumayr, P., and Hagemann, S. E., 2002, Hydrothermal fluid evolution within the Cadillac Tectonic Zone, Abitibi Greenstone Belt, Canada: Relationship to auriferous fluids in adjacent second- and third-order shear zones: Economic Geology, v. 97, p. 1203-1225.
Neumayr, P., Hagemann, S. E., and Couture, J. F., 2000, Structural setting, textures and timing of hydrothermal veins systems in the Val d'or camp, Abitibi, Canada: Implications for the evolution of transcrustal, second- and higher-order fault zones and gold mineralisation: Canadian Journal of Earth Sciences, v. 37, p. 95-115.
Nichols, S., 2003, Structural control, hydrothermal alteration and relative timing of gold mineralisation at the New Celebration gold deposits, Kalgoorlie, Western Australia: Unpub. BSc (Hons) thesis, University of Western Australia, 62 p.
Passchier, C. W., 1994, Structural geology across a proposed terrane boundary in the eastern Yilgarn craton, Western Australia: Precambrian Research, v. 68, p. 43-64.
Passchier, C. W., and Trouw, R. A. J., 1996, Microtectonics, Springer.

Pichavant, M., Ramboz, C., and Weisbrod, A., 1982, Fluid immiscibility in natural processes: Use and misuse of fluid inclusion data 1. Phase equilibria analysis - a theoretical and geometrical approach: Chemical Geology, v. 37, p. 1-27.
Potter, R. W., 1977, Pressure corrections for fluid inclusion homogenization temperatures based on the volumetric properties of the system H_2O-NaCl: Journal of Research of the U.S Geological Survey, v. 5, p. 603-607.
Ramboz, C., Pichavant, M., and Weisbrod, A., 1982, Fluid immiscibility in natural processes: Use and misuse of fluid inclusion data II. Interpretation of fluid inclusion data in terms of immiscibility: Chemical Geology, v. 37, p. 29-48.
Robert, F., 1989, Internal structure of the Cadillac tectonic zone southeast of Val d'or, Abitibi greenstone belt, Quebec: Canadian Journal of Earth Sciences, v. 26, p. 2661-2675.
Robert, F., 1990, An overview of gold deposits in the eastern Abitibi subprovince: Canadian Institute of Mining and Metallurgy Special Volume, v. 43, p. 93-105.
Roedder, E., 1963, Studies of fluid inclusions II: Freezing data and their intepretation: Economic Geology, v. 58, p. 167-211.
Roedder, E., 1984, Fluid Inclusions, Mineralogical Society of America, 644 p.
Shepherd, T. J., Rankin, A. H., and Alderton, D. H. M., 1985, A practical guide to fluid inclusion studies: Glasgow, Blackie, 239 p.
Sorby, H. C., 1858, On the microscopical structure of crystals indication the origin of rocks and minerals: Quarterly Journal of the Geological Society of London, v. 14, p. 453-500.
Swager, C., 1989, Structure of Kalgoorlie greenstones - Regional deformation history and implications for the structural setting of the Golden Mile gold deposits, Geological Society of Western Australia Report 25, p. 59-84.
Swager, C., 1997, Tectono-stratigraphy of late Archaean greenstone terranes in the southern Eastern Goldfields, Western Australia: Precambrian Research, v. 83, p. 11-42.
Swager, C., and Griffin, T. J., 1990, Geology of the Archaean Kalgoorlie Terrane (northern and southern sheets), Western Australian Geological Survey, 1:250,000 Geological Map.
Swager, C., and Nelson, D. R., 1997, Extensional emplacement of a high-grade granite gneiss complex into low-grade greenstones, Eastern Goldfields, Yilgarn Craton, Western Australia: Precambrian Research, v. 83, p. 203-219.
Swanenberg, H. E. C., 1979, Phase equilibria in carbonic systems, and their application to freezing studies of fluid inclusions: Contributions to Mineralogy and Petrology, v. 68, p. 303-306.
Thiery, R., van den Kerkhof, A. M., and Dubessy, J., 1994, vX properties modeling of CH_4-CO_2 and CO_2-N_2 fluid inclusions ($T<31°C$, $P<400$ bar): European Journal of Mineralogy, v. 6, p. 753-771.
Weinberg, R. F., Moresi, L., and van der Borgh, P., 2003, Timing of deformation in the Norseman-Wiluna Belt, Yilgarn Craton, Western Australia: Precambrian Research, v. 120, p. 219-239.
Wilkinson, J. J., 2001, Fluid inclusions in hydrothermal ore deposits: Lithos, v. 55, p. 229-272.
Wilkinson, L., Cruden, A. R., and Krogh, T. E., 1999, Timing and kinematics of post-Timiskaming deformation within the Larder Lake-Cadillac deformation zone, southwest Abitibi greenstone belt, Ontario, Canada: Canadian Journal of Earth Sciences, v. 36, p. 627-647.
Williams, H., 1994, The lithological setting and controls on gold mineralization in the Southern Ore Zone of the Hampton-Boulder gold deposit, New Celebration Gold Mine, Western Australia: Unpub. BSc (Hons) thesis, University of Western Australia.
Williams, P. R., and Currie, K. L., 1993, Character and regional implication of the sheared Archaean granite-greenstone contact near Leonora, Western Australia: Precambrian Research, v. 62, p. 343-365.
Witt, W. K., 1991, Regional metamorphic controls on alteration assemblages associated with gold mineralisation in the Eastern Goldfields Province, Western Australia: Implications for the timing and origin of Archean lode-gold deposits: Geology, v. 19, p. 982-985.